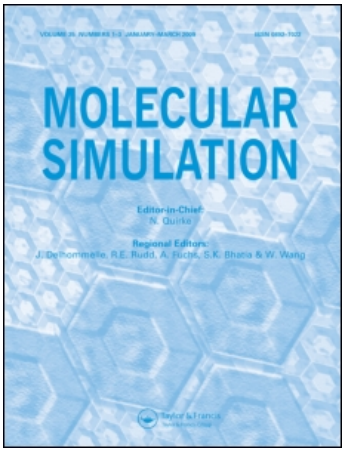

Molecular Simulation
Publication details, including instructions for authors and subscription information:
http://www.informaworld.com/smpp/title~content=t713644482

Modelling of the mechanical and mass transport properties of auxetic molecular sieves: an idealised organic (polymeric honeycomb) host-guest system

A. Alderson[a]; P. J. Davies[a]; M. R. Williams[a]; K. E. Evans[b]; K. L. Alderson[a]; J. N. Grima[c]
[a] Centre for Materials Research and Innovation, The University of Bolton, Bolton, UK [b] Department of Engineering, The University of Exeter, Exeter, UK [c] Department of Chemistry, University of Malta, Msida, Malta

To cite this Article Alderson, A. , Davies, P. J. , Williams, M. R. , Evans, K. E. , Alderson, K. L. and Grima, J. N.(2005) 'Modelling of the mechanical and mass transport properties of auxetic molecular sieves: an idealised organic (polymeric honeycomb) host-guest system', Molecular Simulation, 31: 13, 897 — 905
To link to this Article: DOI: 10.1080/08927020500385852
URL: http://dx.doi.org/10.1080/08927020500385852

Molecular Simulation, Vol. 31, No. 13, 15 November 2005, 897–905

Taylor & Francis
Taylor & Francis Group

Modelling of the mechanical and mass transport properties of auxetic molecular sieves: an idealised organic (polymeric honeycomb) host–guest system

A. ALDERSON†*, P. J. DAVIES†, M. R. WILLIAMS†, K. E. EVANS‡, K. L. ALDERSON† and J. N. GRIMA¶

†Centre for Materials Research and Innovation, The University of Bolton, Deane Road, Bolton BL3 5AB, UK
‡Department of Engineering, The University of Exeter, North Park Road, Exeter EX4 4QF, UK
¶Department of Chemistry, University of Malta, Msida MSD 06, Malta

(Received August 2005; in final form September 2005)

Force field-based simulations have been employed to model the mechanical properties of a range of undeformed molecular polymeric honeycombs having conventional and re-entrant hexagon pores. The conventional and re-entrant hexagon honeycombs are predicted to display positive and negative in-plane Poisson's ratios, respectively, confirming previous simulations. The structure, and mechanical and mass transport properties of a layered re-entrant honeycomb ((2,8)-reflexyne) were studied in detail for a uniaxial load applied along the x_2 direction. The mechanical properties are predicted to be stress- (strain-) dependent and the trends can be interpreted using analytical expressions from honeycomb theory. Transformation from negative to positive Poisson's ratio behaviour is predicted at an applied stress of $\sigma_2 = 2$ GPa. Simulations of the loading of C_{60} and C_{70} guest molecules into the deformed layered (2,8)-reflexyne host framework demonstrate the potential for tunable size selectivity within the host framework. The entrapment and release of guest molecules is attributed to changes in the size and shape of the pores in this host–guest system.

Keywords: Auxetic; Negative Poisson's ratio; Molecular honeycombs; Mass transport; Modelling

1. Introduction

Laser-ablated macroscale auxetic (negative Poisson's ratio [1]) polymeric honeycombs have previously been used to demonstrate enhanced cleanable or tunable filter performance due to the auxetic effect [2–5]. This initial work was subsequently extended to auxetic 3D foam filters [5] and to an auxetic zeolite molecular sieve system [5,6,7]. The enhancements arise due to the increased pore size and/or shape change associated with the high volume change for an auxetic material placed under uniaxial load. This is shown schematically in figure 1.

At the molecular level, the entrapment and release scheme depicted in figure 1 leads to potentially interesting possibilities in the controlled release of active agents such as drug molecules and enzymes. A number of auxetic materials are known where the effect is due to molecular-level structural features and deformation mechanisms [8,9] and several theoretical molecular-level auxetic structures have been proposed [1–14].

The theoretical structures include molecular-level polymeric networks [1,13,14] based on the macroscale polymeric honeycomb geometries employed in the original demonstration of beneficial filter performance [3]. Furthermore, the molecular honeycombs have pore dimensions of the order of the diameters of C_{60} and C_{70} "buckyballs" and so the molecular honeycomb–buckyball systems provide a molecular-level host–guest analogue to the previous macroscale honeycomb–glass bead host–guest system studied experimentally and theoretically [3]. They also provide highly idealised systems with which to address current concerns over the mass transport of potentially harmful (toxic) fullerene (and other) nanoparticles [15].

Here, we report on the use of force field-based simulations of the mechanical and mass transport properties of theoretical auxetic polymeric molecular honeycombs with the aim of increasing the understanding of structure–property relationships in auxetic nanomaterials. In a companion paper, we report on a similar study for an inorganic auxetic molecular sieve system [7].

*Corresponding author. Tel.: +44-1204-903513. Fax: +44-1204-370916. Email: a.alderson@bolton.ac.uk

Molecular Simulation
ISSN 0892-7022 print/ISSN 1029-0435 online © 2005 Taylor & Francis
http://www.tandf.co.uk/journals
DOI: 10.1080/08927020500385852

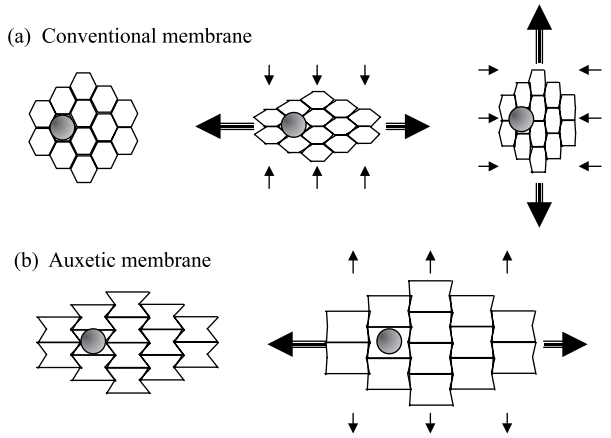

Figure 1. Schematic view of particulate de-fouling capabilities of auxetic and non-auxetic honeycomb membrane filters. Both honeycombs deform by 'hinging' of the cell walls in response to an applied load.

2. Molecular honeycomb networks

Two-dimensional polymeric nanostructures were selected based on the previously proposed [1,13] analogues to the macroscale honeycombs known to enable the design of a negative Poisson's ratio structure through the appropriate choice of geometry and deformation mechanism (see, e.g. figure 1). Figure 2a shows a 5 × 3 unit cells extended molecular network analogous to the conventional honeycomb shown in figure 1a. Figure 2b shows the molecular sub-unit of the analogue to the re-entrant honeycomb shown in figure 1b. The networks consist of branches ("arms") of acetylene groups joined by benzene rings at the junctions. In the re-entrant case, three arms are connected to adjacent benzene ring carbon atoms. The conventional honeycomb geometry is realised when the three arms are connected to alternate benzene ring carbon atoms. The naming convention [1] adopted for the conventional and re-entrant molecular honeycomb networks is (*n*,*m*)-flexyne and (*n*,*m*)-reflexyne, respectively, where *n* and *m* are the respective number of acetylene links in the diagonal and vertical branches. The conventional molecular honeycomb in figure 2a is, therefore, (1,2)-flexyne, and the re-entrant molecular honeycomb in figure 2b is (1,4)-reflexyne.

The choice of the (*n*,*m*)-flexyne and (*n*,*m*)-reflexyne family of 2D organic network structures enables the building of the networks and the calculation of their elastic constants within the molecular modelling software to be verified against previous molecular mechanics simulations [1,13]. These molecular honeycomb nanostructures also possess pore sizes of the order of the diameters of C_{60} and C_{70} "buckyballs". It is possible, therefore, to select a molecular honeycomb and buckyball host–guest system with which to perform combined molecular mechanics and Monte-Carlo simulations of the mass transport properties of an auxetic molecular honeycomb over a range of applied stress.

3. Modelling methodology

A Silicon Graphics O2 workstation running the *Cerius*^{2} Molecular Modelling software (Accelrys, Version 4.6) was employed. The simulations employed the Dreiding force field (Version 2.21) suitable for predicting a range of polymeric material properties [16]. The Dreiding force field is often used for united atom calculations where hydrogen atoms are incorporated within the carbon atom type, but in this work specific atom types were employed

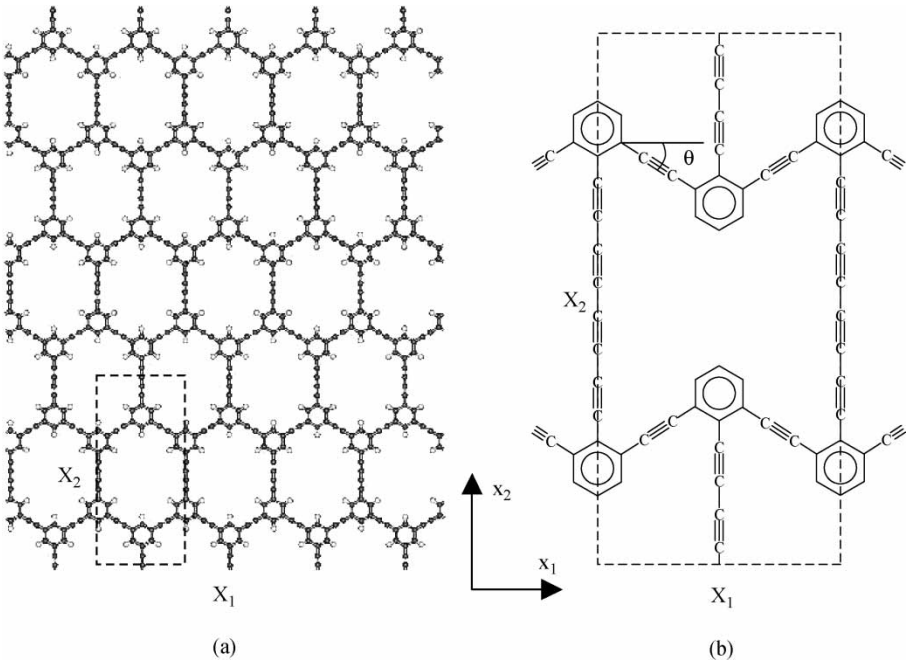

Figure 2. (a) Theoretical 2D conventional molecular honeycomb network—'(1,2)-flexyne'; (b) sub-unit of theoretical auxetic molecular network—'(1,4)-reflexyne'.

for the carbon atoms and the hydrogen atoms to give an all C–H system.

The starting unit-cell structures for the 2D polymeric molecular honeycomb networks were built using the 3D Sketcher and Crystal Builder modules within *Cerius*^{2} and were based on predicted geometries from previous molecular mechanics simulations [13]. Neutral atoms were employed, i.e. charges were not assigned. This effectively builds an idealised neutrally charged 3D crystal of layers of 2D planar networks suitable for the mass transport simulations. The out-of-plane lattice parameter was set between 3.6 and 3.8 Å. This is consistent with the value from previous simulations [13] and represents the inter-plane separation. Periodic boundary conditions were applied and the potential energy of the undeformed structure with P1 unit-cell symmetry was then minimised as a function of the atomic coordinates to the earlier of the default *Cerius*^{2} high convergence criterion (atomic RMS of 0.001 kcal/mol) or 5000 minimisation steps. This step was repeated three times to enable re-calculation of the non-bond list. The inter-plane separation is minimised to ~3.6 Å in all cases.

The second derivative of the energy expression was used to compute the stiffness matrix C, and the on-axis elastic constants were obtained directly from the compliance matrix. The in-plane Poisson's ratios (ν_{ij}) were calculated from the compliance coefficients (s_{ij}) using

$$\nu_{ij} = -\frac{s_{ji}}{s_{ii}} \tag{1}$$

where the subscripts i and j refer to directions x_i and x_j parallel and perpendicular to the loading direction, respectively. The Young's moduli (E_i) were calculated using

$$E_i = \frac{1}{s_{ii}} \tag{2}$$

Deformed structures were modelled for uniaxial applied tensile stress along the x_2 in-plane direction in 0.4 GPa increments within the range of $\sigma_2 \leq 4$ GPa. This size of stress increment is of the order of that used in previous work [13] on these structures and has been shown to be sufficient to yield accurate results [17]. The starting structure at each increment of applied stress was the minimised structure from the previous stress level. The elastic constants calculated directly from the applied stresses and the resultant strains in the minimised deformed structures were used to confirm the elastic constants calculated using the second derivative method.

The simulation of the loading of C_{60} molecules and the simultaneous loading of C_{60} and (slightly larger) C_{70} molecules within the minimised deformed (2,8)-reflexyne layered structures described above was performed using the Dreiding force field. The (2,8)-reflexyne network was selected for the sorption study due to the pore dimensions being similar to the diameters of C_{60} and C_{70} molecules which were, therefore, used as guest molecules in the simulations. Charges were not applied to the sorbate molecules, rendering neutral charges to both the sorbates and the host framework. Simulations were performed on a 3 × 2 unit-cell superlattice of eight layers. The layers were spaced as described above (inter-plane separation of ~3.6 Å) which ensured that the interlayer separation itself did not allow the guest molecules to be accomodated within the overall structure.

All host–guest simulations employed the fixed pressure grand canonical Monte-Carlo method, which allows creation and destruction of sorbate molecules and varies their position and orientation. Creation and destruction probabilities were set equal to ensure microscopic reversibility. Starting values of 1 Å and 50° were employed for the maximum translation and rotation steps, respectively, and these were automatically rescaled during the run to try to minimize the equilibration period. The energy calculation was confined to intermolecular or non-bond energies (i.e. sorbate-framework and sorbate–sorbate interactions), with both the framework and the sorbates held internally rigid during the simulation. Van der Waals energy was calculated by summing all pair interactions within a sphere of radius determined by the interaction cut-off distance. It is important that the interaction cut-off minimises the number of interactions for computational efficiency whilst ensuring sufficient interactions for accuracy. Cut-off distances of the order of 10–20 Å are typical and depend on whether the system being studied is an isolated molecule or cluster (lower cut-off distance) or a periodic crystalline system (longer cut-off distance). Each atom was considered to interact only with its closest neighbour atoms in a periodic box around it, requiring that the cut-off sphere must be smaller than the periodic cell. The choice of an eight-layered 3 × 2 unit-cell superlattice with automated interaction cut-off ensured this requirement was satisfied.

A sorption temperature of 300 K was used throughout. For each simulation, a free volume calculation was carried out to ensure that guest molecules were not placed in areas made inaccessible due to the Van der Waals radii of the atoms in the host structure. Before the energy was calculated, high-energy configurations where any sorbate and framework atoms were closer to each other than half of their Van der Waals radii were rejected. Initial simulations were performed to determine the required number of configurations to ensure equilibrium had been achieved. Consequently, all full simulations were run with 10^5 configurations at each loading level.

4. Results

4.1 Structure and mechanical properties

4.1.1 Undeformed. Table 1 contains the predicted unit-cell lengths, and in-plane Poisson's ratios and Young's moduli for selected undeformed (*n*,*m*)-flexyne and (*n*,*m*)-reflexyne networks. The unit-cell dimensions and elastic constants from a previous molecular modelling study [13] employing the Dreiding force field are also included in

Table 1. Calculated unit-cell lengths and elastic constants (Poisson's ratios and Young's moduli) from Dreiding force-field simulations on selected (*n*,*m*)-flexyne and (*n*,*m*)-reflexyne polymeric honeycomb molecular networks. Previous molecular modelling predictions [13] are included for comparison.

		X_1 (Å)	X_2 (Å)	X_3 (Å)	E_1 (GPa)	E_2 (GPa)	ν_{12}	ν_{21}
(1,2)-flexyne	This work	11.4763	24.6624	3.5626	76	111	0.48	0.698
	Previous work [13]	11.4709	24.6685		75	120	0.46	0.696
(1,4)-flexyne	This work	11.4764	34.2157	3.5781	54.6	140	0.34	0.88
	Previous work [13]	11.4735	34.2045		56.2	160	0.32	0.9
(1,6)-flexyne	This work	11.4765	43.7686	3.5895	43	164	0.27	1.03
	Previous work [13]	11.4671	43.7892		45	220	0.24	0.99
(2,2)-flexyne	This work	15.6182	27.0516	3.5797	29	29	0.85	0.85
	Previous work [13]	15.6314	27.0193		30	30	0.85	0.84
(2,4)-flexyne	This work	15.6181	36.605	3.5911	22	38	0.63	1.11
	Previous work [13]	15.5975	36.6377		23	42	0.6	1.11
(2,6)-flexyne	This work	15.6182	46.1578	3.5997	17	47	0.5	1.36
	Previous work [13]	15.6375	46.1108		19	55	0.47	1.33
(1,5)-reflexyne	This work	11.716	26.1887	3.5645	94	110	−0.33	−0.39
	Previous work [13]	11.7102	26.1698		95	116	−0.29	−0.386
(1,6)-reflexyne	This work	11.717	30.9689	3.5711	80	124	−0.28	−0.44
	Previous work [13]	11.7151	30.9691		84	140	−0.22	−0.42
(2,6)-reflexyne	This work	15.965	28.7588	3.5876	37.2	31	−0.83	−0.69
	Previous work [13]	15.9271	28.6706		35.8	31	−0.80	−0.7
(2,8)-reflexyne	This work	15.9711	38.3261	3.5956	27.9	39	−0.63	−0.887
	Previous work [13]	15.9098	38.1895		31.4	40	−0.57	−0.902

table 1 for comparison. In the previous study, the elastic constants were calculated from the average of the values calculated from the stress–strain (Young's moduli) and transverse strain–longitudinal strain (Poisson's ratio) data for tensile loading of 0.5 GPa and compressive loading of −0.5 GPa.

The calculated unit-cell lengths, Young's moduli and Poisson's ratios are in good agreement with the data from the previous simulations on these networks, verifying the methodology employed in this work. The simulations predict negative Poisson's ratios for the re-entrant ((*n*,*m*)-reflexyne) structures, and positive Poisson's ratios for the conventional hexagonal ((*n*,*m*)-flexyne) structures.

4.1.2 Deformed. A detailed study of the variation of the predicted elastic constants for a range of (*n*,*m*)-flexyne and (*n*,*m*)-reflexyne networks has been performed previously [17] and so this is not repeated here in this work. However, in order to relate the sorption simulation data to the predicted mechanical properties, the variation with tensile loading along the x_2 direction of the Poisson's ratios and Young's moduli of the network selected for study ((2,8)-reflexyne) are shown in figure 3a and b, respectively. For completeness, the elastic constants for both principal in-plane directions are included as a function of applied stress along the x_2 direction in figure 3.

The elastic constants for (2,8)-reflexyne are predicted to vary with applied stress. The in-plane Poisson's ratios for (2,8)-reflexyne fall into three distinct regions of applied stress: (I) negative values for $\sigma_2 < 1.8$ GPa; (II) positive values for $1.8 < \sigma_2 < 3.4$ GPa; and (III) rapidly divergent values of ν_{21} and ν_{12} for $3.4 < \sigma_2 \leq 4$ GPa with ν_{12} tending to a low positive value (~ 0.1) and ν_{21} taking a large positive value (~ 6.6) at $\sigma_2 = 4$ GPa.

In the case of the Young's moduli, the behaviour with applied stress is split into the same three regions of stress:

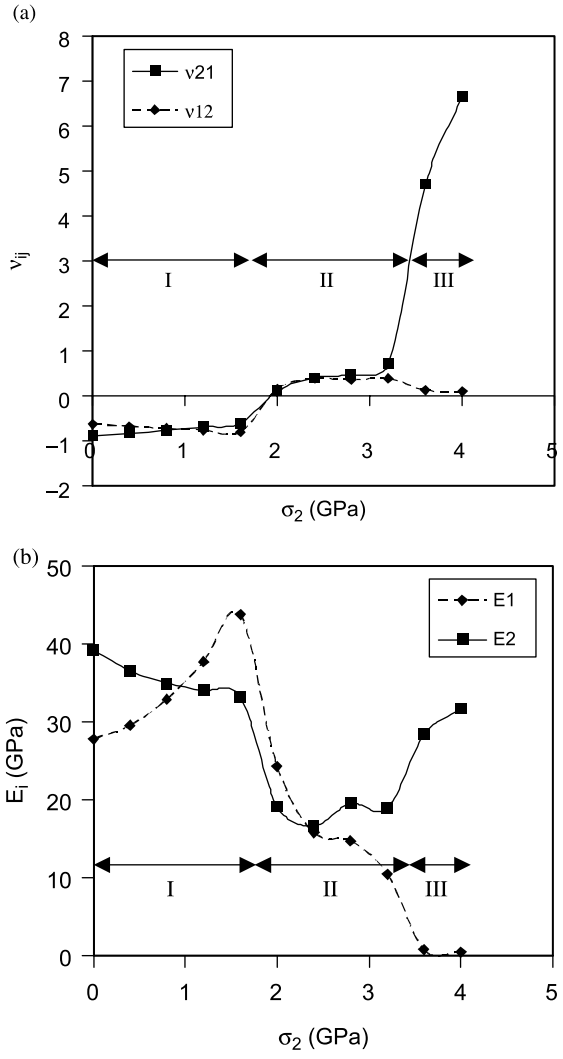

Figure 3. Predicted elastic constants for (2,8)-reflexyne under tensile loading along the x_2 direction: (a) Poisson's ratios (ν_{21} and ν_{12}) vs. applied stress (σ_2); (b) Young's moduli (E_2 and E_1) vs. σ_2.

(I) the low stress region ($\sigma_2 < 1.8$ GPa) where E_2 decreases and E_1 increases with stress; (II) the medium stress region ($1.8 < \sigma_2 < 3.4$ GPa) where E_2 remains approximately constant and E_1 decreases with increasing stress; and (III) the high stress region ($3.4 < \sigma_2 \leq 4$ GPa) where E_2 increases and E_1 decreases (to a very low value ~ 0.5 GPa at $\sigma_2 = 4$ GPa) with stress.

4.2 Sorption properties

Figure 4 shows the calculated C_{60} loading as a function of applied stress in the x_2 direction for the simulations of C_{60} sorption onto the layered (2,8)-reflexyne network. In the undeformed structure, ($\sigma_2 = 0$) the simulations predict no C_{60} molecules are accommodated within the layered (2,8)-reflexyne structure, indicating that the C_{60} guest molecules are too large with respect to the undeformed pore size and shape. However, at $\sigma_2 = 0.4$ GPa the pores of the structure have opened sufficiently to allow C_{60} molecules into the layered network. The loading of C_{60} increases with tensile load up to 3.2 GPa, whereafter the C_{60} loading drops abruptly to 0.

Figure 5 shows a series of "snapshots" of the loading of C_{60} molecules in the layered (2,8)-reflexyne structure at each increment of applied stress along x_2 and is consistent with the data in figure 4.

The predicted C_{70}/C_{60} loading ratio in the simulations of simultaneous loading of C_{60} and C_{70} molecules into the layered (2,8)-reflexyne network as a function of applied stress in the x_2 direction is shown in figure 6. At $\sigma_2 = 0.4$ GPa the C_{70}/C_{60} loading ratio is zero (figure 6), indicating only C_{60} molecules are accommodated within the layered structure (figures 4 and 5). The C_{70} molecules begin to be accommodated within the structure at $\sigma_2 = 0.8$ GPa and the C_{70}/C_{60} loading ratio increases up to $\sigma_2 = 2.4$ GPa. There is a reduction in the C_{70}/C_{60} ratio when $2.4 < \sigma_2 \leq 3.2$ GPa. The sorption simulations on the C_{60}–C_{70}–(2,8)-reflexyne guest–guest–host system,

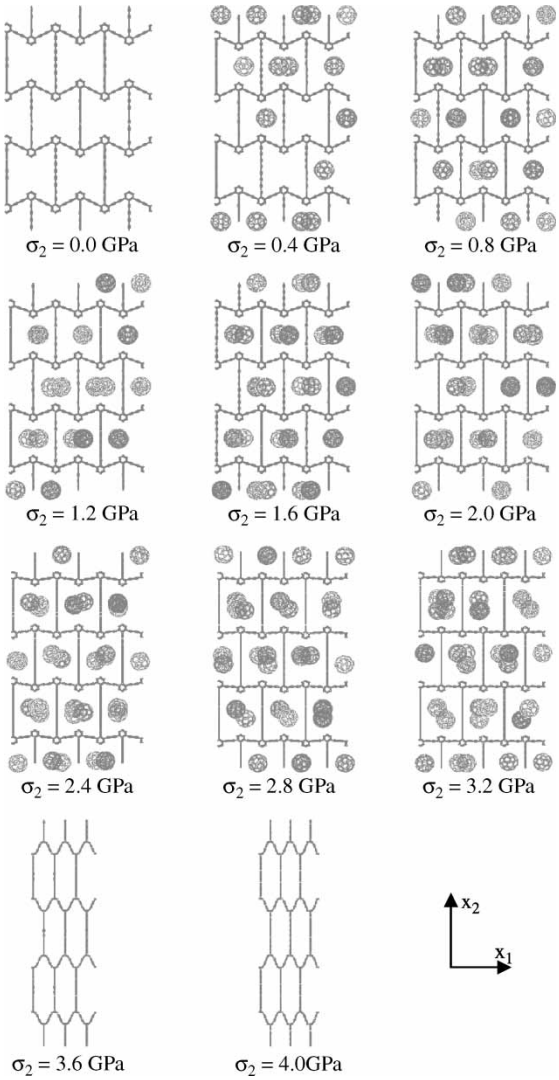

Figure 5. Snapshots of loading of C_{60} molecules within layered (2,8)-reflexyne at each increment of applied stress σ_2.

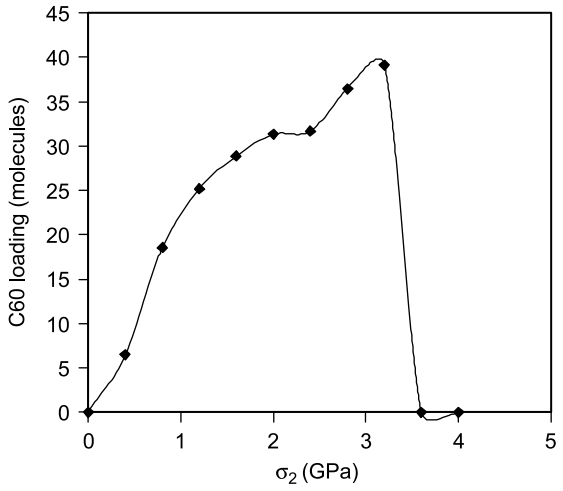

Figure 4. Predicted loading of C_{60} molecules within layered (2,8)-reflexyne vs. σ_2.

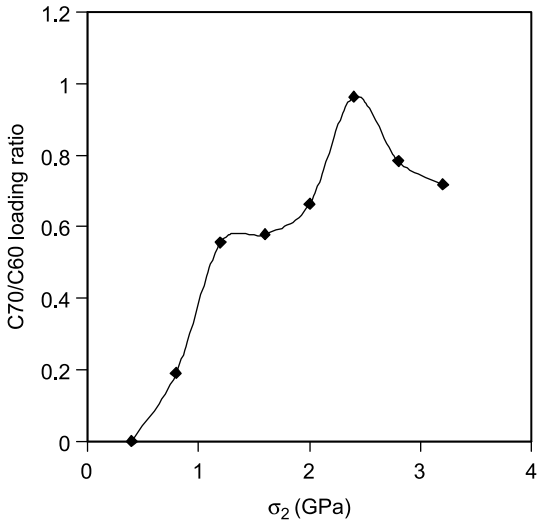

Figure 6. Predicted C_{70}/C_{60} loading ratio within layered (2,8)-reflexyne vs. σ_2.

therefore, confirm size selectivity can be varied in an auxetic molecular sieve system through the application of an applied stress.

5. Discussion

Table 1 shows that the predicted lattice parameters and elastic constants for a range of (*n*,*m*)-flexyne and (*n*,*m*)-reflexyne structures are in good agreement with those predicted previously [13] with the Dreiding force field. Generally, the structures display anisotropic mechanical properties, with the only exception being the (2,2)-flexyne structure having the regular hexagonal honeycomb geometry known to lead to isotropic in-plane properties at the macroscale [18]. The re-entrant structures display auxetic behaviour whereas the conventional hexagonal structures possess positive Poisson's ratios, analogous to the macroscopic honeycomb geometries from which these molecular network structures were designed. However, it has been shown elsewhere that whilst the sign of Poisson's ratio in the molecular honeycombs is well predicted by honeycomb theory applicable to macroscopic honeycombs, the magnitude of Poisson's ratio is not [13]. In order to reproduce in analytical models, the mechanical properties predicted from force-field simulations it has been necessary to include concurrent deformation modes describing flexure, hinging and stretching of the arms of the honeycombs and also to take account of the inhomogeneity of the arms of the honeycombs at the molecular scale [13]. From the previous study, the hinging and/or flexure of the arms is the dominant mode(s) of deformation in the undeformed (*n*,*m*)-flexyne and (*n*,*m*)-reflexyne structures.

The simulations of the variation of mechanical properties of the (2,8)-reflexyne structure with tensile stress along the x_2 direction are in agreement with previous simulations [17] indicating that the properties are stress-(and strain-) dependent (figure 3). In the simulations reported here, strains of the order of 14% are applied at the maximum stress level of $\sigma_2 = 4$ GPa. This level of strain is acceptable in polymer systems; although some caution should be applied as to how realistic the molecular simulations are of the heavily cross-linked network structures studied here in the high stress region. Nevertheless, the simulations provide theoretical polymeric systems with which to study the relationships between structure, mechanical properties and mass transport properties as a function of applied stress.

Strain-dependent, non-linear mechanical properties have been measured and/or predicted in other auxetic materials, including polymeric and metallic foams [19,20], microporous polymers [21,22], and at the molecular level in the α-cristobalite and α-quartz polymorphs of crystalline silica [23], and the all-silica zeolite MFI (ZSM5—$Si_{96}O_{192}$) [7].

Figure 3 also shows that there are two stress levels where $E_1 = E_2$ and $\nu_{12} = \nu_{21}$, indicating that the anisotropic mechanical properties associated with the undeformed (2,8)-reflexyne structure (table 1) have been transformed into in-plane isotropic mechanical properties at these stress levels. At $\sigma_2 \sim 1$ GPa the structure behaves as an isotropic auxetic network, and at $\sigma_2 \sim 2.4$ GPa the structure behaves as an isotropic non-auxetic network.

The simulations predict a stress-induced transition from auxetic to non-auxetic behaviour at $\sigma_2 \sim 2$ GPa (figure 3a). A stress-induced auxetic-to-non-auxetic transition has also been predicted in other molecular-level systems [7,23] and has been observed experimentally in larger-scale auxetic materials [21,22]. It is interesting to note that at $\sigma_2 \sim 2$ GPa the (2,8)-reflexyne structure still has a re-entrant hexagon geometry (figure 5), usually associated with auxetic behaviour, despite now exhibiting positive Poisson's ratio behaviour. Indeed the structure adopts the re-entrant hexagon geometry for tensile loads up to $\sigma_2 \sim 3.2$ GPa.

A re-entrant hexagon geometry can exhibit positive Poisson's ratios when stretching of the honeycomb arms dominates over flexure and hinging of the arms [13,24]. It has been shown previously [13] that stretching is predicted to occur predominantly at the benzene ring and the bond connecting each acetylene arm to the benzene ring junction. At $\sigma_2 \sim 2$ GPa the network has undergone $\sim$6% strain and so the interconnecting vertical arm-junction bonds and associated benzene rings are under severe tensile strain. The strength parameter governing the stretching mode of deformation is inversely proportional to the length of the member undergoing stretching. Hence the severe strain associated with the junctions when $\sigma_2 \sim 2$ GPa will lead to a lowering of the stretching-strength parameter and therefore an increase in the stretching mode, consistent with the predicted positive Poisson's ratio for the re-entrant hexagon geometry at this stress level.

Whilst stretching is, therefore, the dominant mechanism, the alignment of the diagonal arms along the x_1 direction as the stress increases from $\sigma_2 = 2$–3.2 GPa, shown in figure 5, confirms hinging of the arms is also acting as a minor deformation mechanism.

At $\sigma_2 = 3.6$ GPa the (2,8)-reflexyne structure undergoes an abrupt change in geometry to an elongated conventional hexagon geometry, characteristic of a phase transition at this point, and is achieved by the benzene ring junctions undergoing a rotation of 90° out of the x_1–x_2 plane. This change is accompanied by an abrupt change in the mechanical properties, although the Poisson's ratios do not change sign despite the change from re-entrant to conventional hexagon geometry. This implies that stretching of the arms is not the dominant mechanism in the conventional geometry and is probably explained due to the alignment of the diagonal arms towards the x_2 direction being a significant contribution to the overall tensile strain. This will have the effect of reducing the level of tensile strain associated with the benzene ring junctions and, therefore, a recovery of the stretching strength parameter in this case, making the stretching mode more difficult to achieve with respect to flexure and hinging of the arms.

In light of the above discussion, the trends in the molecular modelling data in figure 3 can be interpreted using previously developed analytical model expressions from honeycomb theory [13,18].

In region (I), ($\sigma_2 < 1.8$ GPa) deformation is predominantly due to flexure and/or hinging of the arms of the re-entrant honeycomb network. The analytical expression for the in-plane Poisson's ratios due to arm flexure and/or hinging is:

$$\nu_{12} = \nu_{21}^{-1} = \frac{\cos\theta}{\sin\theta}\frac{X_1}{X_2} \tag{3}$$

where θ is the angle the diagonal arm makes with the horizontal (x_1) direction (shown in figure 2b). The equivalent analytical expressions from honeycomb theory for E_1 and E_2 due to arm flexure and/or hinging are:

$$E_1 = \frac{K_{f/h}}{l^2\sin^2\theta}\frac{X_1}{X_2} \tag{4}$$

$$E_2 = \frac{K_{f/h}}{l^2\cos^2\theta}\frac{X_2}{X_1} \tag{5}$$

where $K_{f/h}$ is the force constant for the flexure or hinging mode and l is the length of a diagonal arm. For the re-entrant network the honeycomb angle is negative and tending towards 0 as $\sigma_2 \rightarrow 1.8$ GPa. Consequently, equation (3) implies ν_{12} and ν_{21} will both be negative with ν_{12} increasing in magnitude and ν_{21} decreasing in magnitude as $\sigma_2 \rightarrow 1.8$ GPa. Equations (4) and (5) indicate E_1 will increase and E_2 will decrease as $\sigma_2 \rightarrow 1.8$ GPa.

Arm flexure and/or hinging is also the dominant deformation mechanism(s) in the high stress region (III) ($3.4 < \sigma_2 \leq 4$ GPa). From figure 5 the structure in region (III) is characterised by a large positive value of θ which increases towards 90° as $\sigma_2 \rightarrow 4.0$ GPa. Hence equation (3) indicates ν_{12} and ν_{21} tend towards low and high positive values, respectively, as $\sigma_2 \rightarrow 4.0$ GPa. Similarly, equations (4) and (5) indicate E_1 and E_2 tend to very low and very high values, respectively, as $\sigma_2 \rightarrow 4.0$ GPa (i.e. $\theta \rightarrow 90°$). The elastic constants predictions from the force-field simulations in the low stress region (I) and high stress region (III) in figure 3 are, therefore, consistent with re-entrant and conventional hexagon honeycombs, respectively, deforming predominantly due to hinging and/or flexure of the arms.

In region (II) ($1.8 < \sigma_2 < 3.4$ GPa), it is suggested that deformation is predominantly due to stretching of the arms of the re-entrant honeycomb network, with hinging of the arms also playing a minor role. The analytical expressions for the in-plane Poisson's ratios and Young's moduli due to arm stretching are:

$$\nu_{12} = -\frac{\sin\theta}{\cos\theta}\frac{X_1}{X_2} \tag{6}$$

$$\nu_{21} = -\frac{\cos\theta\sin\theta}{(2+\sin^2\theta)}\frac{X_2}{X_1} \tag{7}$$

$$E_1 = \frac{K_s}{\cos^2\theta}\frac{X_1}{X_2} \tag{8}$$

$$E_2 = \frac{K_s}{(2+\sin^2\theta)}\frac{X_2}{X_1} \tag{9}$$

where K_s is the force constant for the stretching mode, and equations (6)–(9) assume stretching occurs only at the acetylene arm-benzene ring junction [13]. In the case of deformation due to stretching of a re-entrant network (i.e. a negative value of θ), equations (6) and (7) are independent of the stretching force constant and imply ν_{12} and ν_{21} will both be positive. Equations (8) and (9), on the other hand, depend on both the stretching force constant and the honeycomb angle. As discussed above, we expect K_s will decrease as $\sigma_2 \rightarrow 3.4$ GPa due to the excessive strain at the junction. It is also clear that the honeycomb angle $\theta \rightarrow 0$ as $\sigma_2 \rightarrow 3.4$ GPa due to the minor mechanism of arm hinging (figure 5). The reduction in both K_s and θ as $\sigma_2 \rightarrow 3.4$ GPa both act to decrease E_1 according to equation (8), whereas these two effects tend to oppose each other in equation (9) leading to E_2 remaining approximately constant throughout region (II). Hence, the data in figure 3 for the medium stress region (II) are consistent with deformation due predominantly to stretching of the arms with a minor deformation mechanism due to hinging of the arms.

The simulations of the loading of C_{60} and C_{70} molecules within the layered (2,8)-reflexyne framework show a clear dependency with applied stress along the x_2 direction (figures 4 and 6). This is analogous to the size selectivity demonstrated experimentally in macroscale auxetic honeycomb [2–5] and foam [2,5] filters, and predicted theoretically in an inorganic auxetic zeolite molecular sieve [5,7].

The clear positioning of the C_{60} molecules within the pores in figure 5 confirms that the molecules are accommodated within the layered framework due to the in-plane pore size variations and not as a result of any variation in the interlayer separation that may occur as a result of applied stress.

Considering first the simulation of the loading of C_{60} molecules only (figure 4), the admission of C_{60} molecules within the structure is due to the expansion of the pores both along and transverse to the loading direction as a result of the negative value of ν_{21} in region (I). From the mechanical properties simulations (figure 3a) ν_{21} is positive for tensile stress $\sigma_2 \geq 2$ GPa. However, since the elastic constants were derived from the second derivative of the energy expression, the calculated Poisson's ratios

correspond to instantaneous or incremental values [22]. A positive ν_{21} in region (II) indicates that the X_1 lattice parameter is contracting whilst X_2 is elongating. The contraction of X_1 during region (II) is, however, less than the elongation it undergoes due to the negative ν_{21} in region (I). Hence, in region (II) the structure remains expanded along both the x_1 and x_2 directions with respect to the original undeformed structure and, in fact, the in-plane area ($X_1 \times X_2$) increases with stress throughout both regions (I) and (II). Hence, the C_{60} loading continues to increase with stress during region (II) (figure 4), albeit at a lower rate than for region (I), consistent with the lower rate of volume increase determined by the positive Poisson's ratio in region (II).

For $\sigma_2 \geq 3.2$ GPa the structure adopts the conventional honeycomb geometry and the vertical acetylene arms now act to reject totally the C_{60} molecules.

Considering now, the simulations of simultaneous loading of C_{60} and C_{70} molecules, size selectivity due to the pore dimension changes is evident. For $\sigma_2 = 0.4$ GPa figures 4 and 5 show C_{60} molecules are accommodated within the layered structure, but figure 6 shows the C_{70}/C_{60} loading ratio is zero. Hence, the larger C_{70} molecules are excluded and C_{60} is preferentially selected by the framework structure when $\sigma_2 = 0.4$ GPa. The C_{70} molecules begin to be included within the framework as a result of pore expansion at $\sigma_2 = 0.8$ GPa and the C_{70}/C_{60} loading ratio increases up to $\sigma_2 = 2.4$ GPa. The closing of the vertical acetylene arms as a result of the positive Poisson's ratio for $\sigma_2 \geq 2$ GPa eventually leads to a reduction in the loading of C_{70} molecules (and therefore, the C_{70}/C_{60} ratio) when $2.4 < \sigma_2 \leq 3.2$ GPa.

The simulations on the $C_{60}-C_{70}-$(2,8)-reflexyne guest–guest–host system confirm the presence of a negative Poisson's ratio enhances size selectivity in a molecular sieve material. This was also found in a similar study of a 3D inorganic zeolite host–guest system [6,7]. It is clear in these systems the presence of a negative Poisson's ratio offers greater potential to tune the size of guest molecule to be accommodated within the host structure as a result of the simultaneous increase (decrease) in both in-plane pore dimensions when stretched (compressed).

This and related studies into the potential of auxetic molecular host structures in mass transport processes should lead to the eventual deployment in a range of applications where the entrapment and release of active molecular species are required. Examples include the controlled release of drugs in the biomedical industry, selective entrapment in molecular sieve, catalysis and ion exchange processes in the chemical engineering and nuclear industries, and the control of potentially toxic nanoparticles. The layered honeycomb systems studied here are likely to prove significantly challenging to synthesise. However, progress is being made in other polymeric systems that may have the potential to be synthesised into a useful form, which will bring applications of the type referred to here nearer to reality. A particularly promising candidate is the design of a liquid crystalline polymer system where auxetic behaviour is due to site-connectivity-driven rotation of laterally attached "rods" (mesogens) in a main-chain liquid crystalline polymer containing a series of "rods" connected terminally or laterally, in an alternating fashion, by flexible "spacer" groups [12].

6. Summary

To summarise, force field-based simulations have been performed to predict the mechanical properties of conventional and re-entrant hexagonal molecular polymeric honeycomb networks. The simulations confirm previous simulations which predict the undeformed re-entrant networks possess negative Poisson's ratios, whereas the conventional honeycomb networks possess positive Poisson's ratios. A specific re-entrant honeycomb ((2,8)-reflexyne) was selected for detailed study into the potential for auxetic molecular sieves displaying enhanced size selectivity properties. The mechanical properties of (2,8)-reflexyne are predicted to be stress- (strain-) dependent and include the transformation of negative-to-positive Poisson's ratios at a critical loading stress along the x_2 direction. The predicted trends in the Poisson's ratios and Young's moduli with applied stress can be interpreted using analytical expressions developed previously. Monte-Carlo simulations of the loading of C_{60} molecules and the simultaneous loading of C_{60} and (slightly larger) C_{70} molecules into a layered (2,8)-reflexyne structure indicate the loading is stress dependent. The entrapment and release of guest molecules within the layered honeycomb structure is determined by variations in the pore size and shape. Pore size and shape variation with applied stress can be more easily achieved using a high volume change negative Poisson's ratio structure than a lower volume change positive Poisson's ratio structure.

Acknowledgements

The authors are grateful to the UK's Engineering and Physical Sciences Research Council for funding this work.

References

[1] K.E. Evans, M.M. Nkansah, I.J. Hutchinson, S.C. Rogers. Molecular network design. *Nature*, **353**, 124 (1991).
[2] A. Alderson, K.E. Evans, J. Rasburn, (1999), PCT Patent, No. WO 99/22838.
[3] A. Alderson, J. Rasburn, S. Ameer-Beg, P.G. Mullarkey, W. Perrie, K.E. Evans. An auxetic filter: a tuneable filter displaying enhanced size selectivity or de-fouling properties. *Ind. Eng. Chem. Res.*, **39**, 654 (2000).
[4] J. Rasburn, A. Alderson, S. Ameer-Beg, P.G. Mullarkey, W. Perrie, K.E. Evans. Auxetic structures for variable permeability systems. *AIChE J.*, **47**(11), 2623 (2001).
[5] A. Alderson, J. Rasburn, K.E. Evans, J.N. Grima. Auxetic polymeric filters display enhanced de-fouling and pressure-compensation properties. *Membr. Technol.*, **137**, 6 (2001).

[6] J.N. Grima, R. Jackson, A. Alderson, K.E. Evans. Do zeolites have negative Poisson's ratios? *Adv. Mater.*, **12**(24), 1912 (2000).
[7] A. Alderson, P.J. Davies, K.E. Evans, K.L. Alderson, J.N. Grima. Modelling of the mechanical and mass transport properties of auxetic molecular sieves: an idealised inorganic (zeolitic) host-guest system. *Mol. Simul.*, (2005) submitted.
[8] Y. Yeganeh-Haeri, D.J. Weidner, J.B. Parise. Elasticity of α-cristobalite: a silicon dioxide with a negative Poisson's ratio. *Science*, **257**, 650 (1992).
[9] R.H. Baughman, J.M. Shacklette, A.A. Zakhidov, S. Stafstrom. Negative Poisson's ratios as a common feature of cubic metals. *Nature*, **392**, 362 (1998).
[10] K.W. Wojciechowski. Constant thermodynamic tension Monte-Carlo studies of elastic properties of a two-dimensional system of hard cyclic hexamers. *Mol. Phys.*, **61**, 1247 (1987).
[11] R.H. Baughman, D.S. Galvao. Crystalline networks with unusual predicted mechanical and thermal properties. *Nature*, **365**, 735 (1993).
[12] C. He, P. Liu, A.C. Griffin. Toward negative Poisson ratio polymers through molecular design. *Macromolecules*, **31**, 3145 (1998).
[13] K.E. Evans, A. Alderson, F.R. Christian. Auxetic two-dimensional polymer networks: an example of tailoring geometry for specific mechanical properties. *J. Chem. Soc. Faraday Trans.*, **91**, 2671 (1995).
[14] F.R. Attenborough, K.E. Evans, A. Alderson, B.R. Eggen, M.I. Heggie. Tailoring the elastic constants of two and three dimensional molecular networks. *Proceedings of the 10th International Conference on Deformation, Yield and Fracture of Polymers, Cambridge, UK*, Inst. Matls. 27, (1997).
[15] E. Oberdoster. Manufactured nanomaterials (fullerenes, C_{60}) induce oxidative stress in the brain of juvenile largemouth bass. *Environ. Health Perspect.*, **112**, 1058 (2004).
[16] S.L. Mayo, B.D. Olafson, W.A. Goddard III. Dreiding—a generic force field for molecular simulations. *J. Phys. Chem.*, **94**, 8897 (1990).
[17] M.A. Nkansah, K.E. Evans, I.J. Hutchinson. Modelling the mechanical properties of an auxetic molecular network. *Mod. Simul. Mater. Sci. Eng.*, **2**, 337 (1994).
[18] L.J. Gibson, M.F. Ashby. *Cellular Solids: Structure and Properties*, Pergamon Press, London (1988).
[19] R.S. Lakes. Foam structures with a negative Poisson's ratio. *Science*, **235**, 1038 (1987).
[20] J.B. Choi, R.S. Lakes. Nonlinear properties of metallic cellular materials with a negative Poisson ratio. *J. Mater. Sci.*, **27**, 5375 (1992).
[21] B.D. Caddock, K.E. Evans. Microporous materials with negative Poisson's ratios. I. Microstructure and mechanical properties. *J. Phys. D: Appl. Phys.*, **22**, 1877 (1989).
[22] K.L. Alderson, A. Alderson, K.E. Evans. The interpretation of the strain-dependent Poisson's ratio in auxetic polyethylene. *J. Strain Anal.*, **32**, 201 (1997).
[23] N.R. Keskar, J.R. Chelikowsky. Structural properties of nine silica polymorphs. *Phys. Rev. B*, **46**, 1 (1992).
[24] I.G. Masters, K.E. Evans. Models for the elastic deformation of honeycombs. *Compos. Struct.*, **35**, 403 (1997).